Design of silicon waveguides integrated with 2D graphene oxide films for Kerr nonlinear optics

Yuning Zhang, Jiayang Wu, Yang Qu, Linnan Jia, Baohua Jia, and David J. Moss

Y. Zhang, Dr. J. Wu, Y. Qu, L. Jia, and Prof. D. J. Moss
Optical Sciences Centre
Swinburne University of Technology
Hawthorn, VIC 3122, Australia
E-mail: jiayangwu@swin.edu.au, bjia@ swin.edu.au, dmoss@swin.edu.au

Prof. B. Jia
Centre for Translational Atomaterials
Swinburne University of Technology
Hawthorn, VIC 3122, Australia

Abstract

The Kerr nonlinear optical performance of silicon nanowire waveguides integrated with 2D layered graphene oxide (GO) films is theoretically studied and optimized based on experimentally measured linear and nonlinear optical parameters of the GO films. The strong mode overlap between the silicon nanowires and highly nonlinear GO films yields a significantly enhanced Kerr nonlinearity for the hybrid waveguides. A detailed analysis for the influence of waveguide geometry and GO film thickness on the propagation loss, nonlinear parameter, and nonlinear figure of merit (FOM) is performed. The results show that the effective nonlinear parameter and nonlinear FOM can be increased by up to ≈52 and ≈79 times relative to bare silicon nanowires, respectively. Self-phase modulation (SPM)-induced spectral broadening of optical pulses is used as a benchmark to evaluate the nonlinear performance, examining the trade-off between enhancing Kerr nonlinearity and minimizing loss. By optimizing the device parameters to balance this, a high spectral broadening factor of 27.6 can be achieved – more than 6 times that achieved in previous experiments. Finally, the influence of pulse chirp, material anisotropy, and the interplay between saturable absorption and SPM is also discussed. These results provide useful guidance for optimizing the Kerr nonlinear optical performance of silicon waveguides integrated with 2D layered GO films.

Keywords: 2D materials, silicon photonics, graphene oxide, Kerr nonlinearity.

1. Introduction

Third-order nonlinear optical processes, including self-phase modulation (SPM), cross phase modulation (XPM), four-wave mixing (FWM), third harmonic generation (THG), and others [1, 2], have formed the basis for all-optical signal generation and processing, which can achieve ultrahigh processing speed without the need to convert the optical signal to the electrical domain (or vice versa) [3-5]. This has underpinned many applications in telecommunications [6], metrology [7], astronomy [8], ultrafast optics [9], quantum photonics [10], and others [11-13].

Realizing nonlinear optical devices in integrated photonic chips would reap the greatest benefits in terms of device footprint, scalability, stability, and mass production. Although silicon has been a dominant platform for integrated photonic chips [14-19], its strong two-photon absorption (TPA) in the near-infrared telecom wavelength band significantly limits its nonlinear performance [1, 2]. Even if the free carriers generated by TPA are swept out by p-i-n junctions [20], silicon's relatively poor intrinsic nonlinear figure of merit (FOM) in the telecom band is below what is needed to achieve superior nonlinear performance [21-23]. In response to this, other complementary metal-oxide-semiconductor (CMOS) compatible platforms have been explored for nonlinear optics, such as silicon nitride (SiN) [24, 25] and Hydex [26 - 45]. However, while these platforms have negligible TPA, they also have a comparatively low Kerr nonlinearity [2, 26].

To overcome these limitations, two-dimensional (2D) materials that exhibit an ultrahigh optical nonlinearity, such as graphene [46, 47], graphene oxide (GO) [48, 49], black phosphorus [50, 51], and transition metal dichalcogenides (TMDCs) [52, 53], have been integrated onto chips to enhance the nonlinear optical performance. Amongst the different 2D materials, GO has become highly promising due to its ease of preparation as well as flexibility in tuning its material properties [54-60]. Previously, GO has been shown to have a giant Kerr nonlinearity – about 4 orders of magnitude higher than silicon [58, 61]. Moreover, GO has a

large bandgap (> 2 eV [54, 62]) that yields a linear absorption that is over 2 orders of magnitude lower than graphene at infrared wavelengths [63] as well as low TPA in the telecom band [62, 64]. Based on this, enhanced SPM in GO-coated silicon nanowires [48] and FWM in GO-coated SiN and Hydex devices have all been demonstrated [49, 63, 65]. An even more appealing advantage of GO is the ability to precisely control the film thickness, size, and position on integrated chips via large-area, transfer-free, layer-by-layer coating methods together with standard lithography and lift-off processes [62, 65, 66]. In contrast to the imprecise, largely unrepeatable, and unstable approach of mechanical layer transfer processes that have been widely used for other 2D materials such as graphene and TMDCs [67, 68], this method enables cost-effective, large-scale, and highly precise integration of 2D layered GO films on a chip, representing a significant advance towards manufacturable integrated photonic devices incorporating 2D materials [60].

Recently [48], we demonstrated an enhanced Kerr nonlinearity in silicon-on-insulator (SOI) nanowires integrated with 2D layered GO films, verified through SPM measurements with picosecond optical pulses. We achieved a maximum spectral broadening factor (BF) of 4.34 for an SOI nanowire with a patterned GO film. In this paper, we fully analyse and optimize the Kerr nonlinear optical performance of GO-coated SOI nanowires based on experimentally measured linear and nonlinear optical parameters of the GO films. We investigate the influence of waveguide geometry and GO film thickness on the propagation loss, nonlinear parameter, and nonlinear FOM. By increasing the mode overlap with GO films, we show that the effective nonlinear parameter and nonlinear FOM of the hybrid waveguides can be increased by up to ≈52 and ≈79 times with respect to bare SOI nanowires, respectively. We find that this needs to be balanced with an accompanying increase in linear loss, and use SPM-induced spectral broadening of the optical pulses to examine the trade-off between enhancing the Kerr nonlinearity and minimizing loss. By changing the device parameters to balance this trade-off, we achieve a high spectral BF of 27.6, more than 6 times higher than

what has been achieved experimentally. Finally, we discuss the influence of pulse chirp, material anisotropy, and the interplay between saturable absorption (SA) and SPM on the Kerr nonlinear optical performance. These results highlight the significant potential to improve on experimental results [48] and provide detailed solutions for optimizing the Kerr nonlinear performance of SOI nanowires integrated with 2D layered GO films.

2. 2D GO films and device structure

Figure 1(a) shows schematics of the atomic structures and bandgaps of graphene and GO. As compared with graphene, GO provides more flexibility to tailor its material properties by manipulation of the oxygen-containing functional groups (OFGs) in the basal plane and sheet edges, including epoxy, hydroxyl, carbonyl and carboxyl groups [54, 69]. Also, in contrast to graphene that has a metallic behavior with zero bandgap, GO has a large bandgap > 2 eV [54, 62] that yields both low linear light absorption and TPA in the telecom band, which are highly desirable for Kerr nonlinear processes such as FWM and SPM [60]. **Figure 1(b)** shows a schematic of an SOI nanowire waveguide integrated with a GO film. The fabrication of the SOI nanowire can be achieved via either deep ultraviolet photolithography or e-beam lithography followed by inductively coupled plasma etching, all of which are mature silicon device fabrication technologies [19, 70]. The GO film coating, with a thickness of ~2 nm per layer [48], can be achieved using solution-based methods that yield layer-by-layer film deposition [62, 63, 66]. As compared with the sophisticated transfer processes for other 2D materials such as graphene and TMDCs [71, 72], these coating methods enable transfer-free and conformal film coating, with high fabrication stability, repeatability, precise control of the film thickness (i.e., number of layers), and extremely good film attachment onto integrated photonic devices [60]. Precise control of the film length and coating position can be achieved by patterning the film with standard lithography and lift-off processes [65, 66]. This, together with the accurate control of the film thickness, allows the optimization of the Kerr nonlinear performance by adjusting the film thickness, length, and coating position.

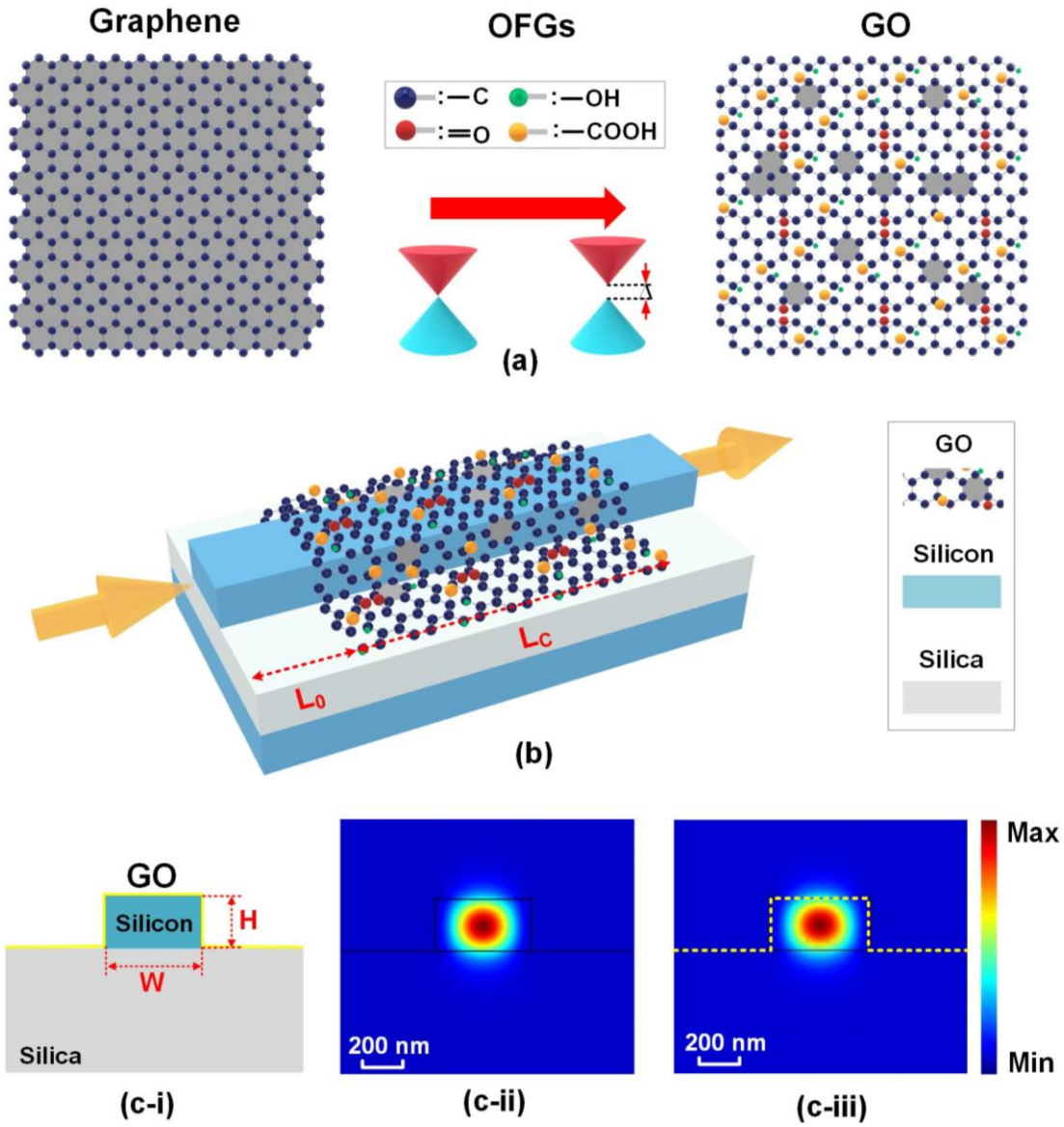

Figure 1. (a) Schematics of atomic structures and bandgaps of graphene and GO. (b) Schematic illustration of a GO-coated SOI nanowire. (c-i) Schematic illustration of cross section of a SOI nanowire conformally coated with 1 layer of GO. (c-ii) TE mode profile for bare SOI nanowire. (c-iii) TE mode profile corresponding to the hybrid waveguide in (c-i). The definitions of L_0, L_c, W, and H are given in Table I.

Figure 1(c-i) shows the schematic cross section of a hybrid waveguide with 1 layer of GO, while **Figures 1(c-ii)** and **(c-iii)** show the transverse electric (TE) mode profile for a bare SOI nanowire and a GO-coated SOI nanowire with the same waveguide geometry. The interaction between the film and waveguide evanescent field excites the nonlinear optical response of the highly nonlinear GO film. **Table I** shows the definition of the parameters that we use to investigate the Kerr nonlinear optical performance of the GO-coated SOI nanowires, including the waveguide dimensions (W and H), GO film parameters (N, L_c and L_0), and

pulsed laser parameters (*PE* and C_0). Following our previous experimental measurements [48, 49, 66], the GO film thickness is assumed to be proportional to *N*, with a thickness of 2 nm per layer. We assume that the input pulse shape has a Gaussian profile:

$$A=\sqrt{P_0}\cdot exp[-\frac{1}{2}(1+iC_0)(\frac{t}{T_0})^2] \quad (1)$$

where P_0 is the pulse peak power, C_0 is the initial chirp, and T_0 is the pulse width (the half-width at 1/*e* intensity). The corresponding pulse energy (*PE*) can be described as

$$PE = P_0 \cdot T_0 \quad (2)$$

Table I. Definitions of parameters of waveguides dimension, GO film, and pulsed laser.

Waveguide dimension	Height		Width
Parameters	*H*		*W*
GO film	GO layer number	Coating length	Uncoated length before GO segment
Parameters	*N*	L_c	L_0
Pulse laser	Pulse energy (coupled into the waveguide)		Chirp
Parameters	*PE*		C_0

In the following sections, we first investigate the influence of waveguide geometry (*W*, *H*) and GO film thickness (*N*) on the linear and nonlinear loss of the hybrid waveguides in Section 3, followed by their effect on the effective nonlinear parameter and nonlinear FOM in Section 4. In Section 5, SPM-induced spectral broadening of optical pulses is investigated to illustrate the trade-off between optimizing the nonlinear FOM and minimizing linear loss. Using the results of Sections 3 and 4, we optimize the spectral broadening in GO-coated SOI nanowires by adjusting the device parameters such as waveguide geometry (*W*, *H*), layer number (*N*), pattern length (L_c), and coating position (L_0). Finally, we discuss the influence of loss, pulse chirp, material anisotropy, and the interplay between SA and SPM on the Kerr nonlinear performance in Section 6.

3. Linear and nonlinear loss

In this section, we investigate the linear and nonlinear loss of GO-coated SOI nanowires with different waveguide geometries (*W*, *H*) and GO film thickness (*N*). **Figure 2(a)** shows the in-plane refractive index (*n*) and extinction coefficient (*k*) of GO (at 1550 nm) versus layer number *N*, measured by spectral ellipsometry. The *k* slightly increases with layer number *N*, varying from 0.0079 for $N = 1$ to 0.0091 for $N = 20$, mainly induced by scattering loss stemming from film unevenness and imperfect contact between the multiple GO layers. Note that the *k* for GO is over two orders of magnitude lower than that of graphene, highlighting its low linear light absorption and strong potential for high-performance nonlinear photonic devices. In principle, GO films with a bandgap > 2 eV should have negligible absorption at telecom wavelengths. Therefore, the *k* of GO, unlike graphene, is not fundamental but rather can be reduced by optimizing film fabrication processes. For the film refractive index *n*, in contrast to the layer dependent *k*, we assume that it is independent of the layer number *N*, consistent with the observation in **Figure 2(a)**.

Figures 2(b-i) and **(b-ii)** depict the linear propagation loss of the hybrid waveguides versus layer number (*N*), first for different waveguide heights (*H*) at a fixed width (*W*) and then for different widths (*W*) at a fixed height (*H*). The propagation loss was calculated using Lumerical FDTD commercial mode solving software with the *n*, *k* of layered GO films from **Figure 2(a)**. We used the propagation loss for bare (uncoated) waveguides from previously fabricated SOI devices [48, 73]. We chose the transverse electric (TE) polarization because it supports an in-plane interaction between the evanescent field and film, which is much stronger than the out-of-plane interaction due to the large optical anisotropy of 2D materials [46, 66, 68]. In **Figures 2(b-i) and (b-ii)**, the propagation loss is seen to increase with layer number N − a combined result of both increased *k* and GO mode overlap. The propagation loss decreases with waveguide height *H* and width *W*, which shows the opposite trend to its

change with layer number *N*, reflecting an increased GO mode overlap in SOI nanowires that feature smaller waveguide dimensions.

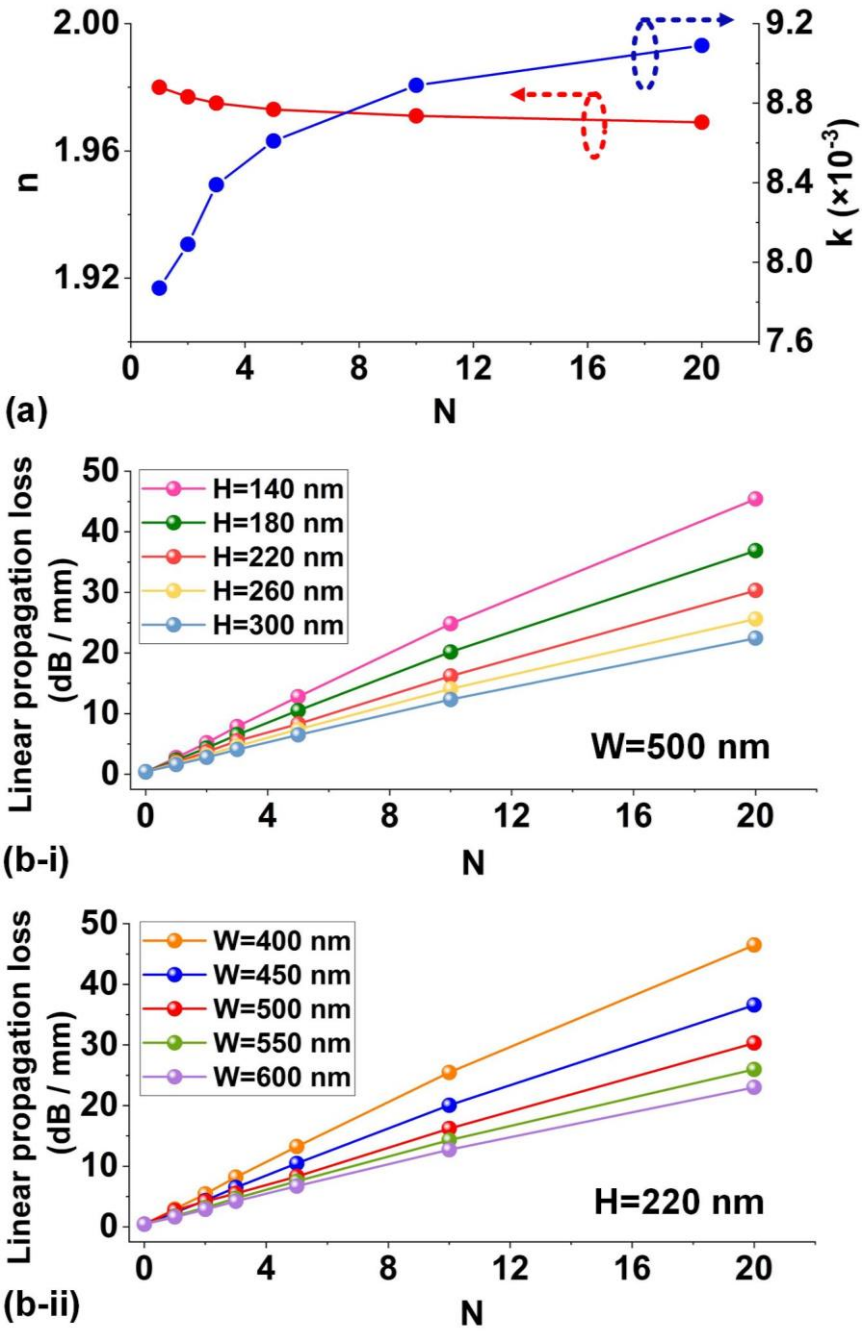

Figure 2. (a) Refractive index *n* and extinction coefficient *k* of GO versus layer number *N*. (b) Linear propagation loss versus *N* for GO-coated SOI nanowires with (i) various *H* when *W* = 500 nm and (ii) various *W* when *H* = 220 nm. The points at *N* = 0 correspond to the results for bare SOI nanowires.

Figure 3(a) depicts the nonlinear loss arising from TPA and free carrier absorption (FCA) of silicon versus pulse energy (*PE*) for the bare SOI nanowires, (i) for different heights (*H*) at a fixed width (*W*) and (ii) for different widths (*W*) at a fixed height (*H*). The pulsed laser

parameters are: pulse width T_0 = 3.9 ps and initial chirp C_0 = -0.3 – taken from our previous experiments [48]. The *PE* varies from 0.38 pJ to 51.5 pJ, corresponding to a varied peak power from 0.1 W to 13.2 W. The TPA and FCA loss was calculated based on [74]:

$$\alpha_{TPA\text{-}Si} + \alpha_{FCA\text{-}Si} = \frac{\beta_{TPA,\,Si}}{A_{eff}} |A(z,\,t)|^2 + \sigma N_c \tag{3}$$

where $\beta_{TPA,\,Si}$ = 5 × 10^{-12} m/W and σ = 1.45 × 10^{-21} m are the TPA and FCA coefficients of silicon, respectively, $A(z,\,t)$ is the slowly varying temporal envelope of the optical pulse along the waveguide (i.e., z axis), and A_{eff} is the effective mode area. N_c is the free carrier density given by [74]:

$$\frac{\partial N_c(z,t)}{\partial t} = \frac{\beta_{TPA,\,Si}}{2\hbar\omega} \cdot \frac{|A(z,t)|^4}{A_{eff}^2} - \frac{N_c(z,t)}{\tau_c} \tag{4}$$

where $\hbar$ is Planck's constant, ω is the angular frequency, and τ_c = ~1 ns is the effective carrier lifetime. When T_0 (e.g., 3.9 ps) is much shorter than τ_c, the τ_c term in **Eq. (4)** can be ignored as the generated free carriers do not have enough time to recombine within the pulse duration [72, 74]. The loss in **Figure 3(a)** decreases with waveguide height H and width W, indicating a stronger TPA and FCA in SOI nanowires that have smaller waveguide dimensions.

As noted previously, the TPA and FCA of GO is very low at near-infrared wavelengths [61, 63] and so the nonlinear loss of GO is dominated by SA arising from the ground-state bleaching of the sp^2 domain with a typical energy gap of ~0.5 eV [58, 61, 75]. **Figure 3(b)** shows the SA loss of the GO films for the hybrid waveguides with different waveguide geometries (H and W) but the same GO film parameters of N = 10 and L_c = 0.4 mm. The SA loss was calculated via [76, 77] :

$$\alpha_{SA\text{-}GO} = \alpha_{sat} / (1 + \frac{\eta |A|^2}{I_{sat}}) \tag{5}$$

where α_{sat} is the SA coefficient, I_{sat} is the saturation intensity, and η is the GO mode overlap. In our calculations, the layer dependent α_{sat} and I_{sat} were obtained from experimental results

[48] and η was calculated via COMSOL Multiphysics. Here, α_{sat} and I_{sat} are determined by the film properties. Given the broadband response of 2D layered GO films [66], the SA of GO was assumed to be wavelength independent. In **Figure 3(b)**, the SA loss becomes more significant as the waveguide height H and width W both decrease. This mainly results from an increase in η, slightly offset by a decrease in pulse energy PE at the start of the GO coated segments (resulting from an increase in linear propagation loss in **Figure 2**). **Figure 3(c)** shows the SA loss versus pulse energy PE, for (i) different layer numbers N at a fixed coating length of L_c = 0.4 mm and (ii) different coating lengths L_c at a fixed layer number of N = 10. It is clear that SA in the films becomes more significant as the layer number N and coating length L_c both increase, reflecting more significant SA in the hybrid waveguides with thicker and longer films.

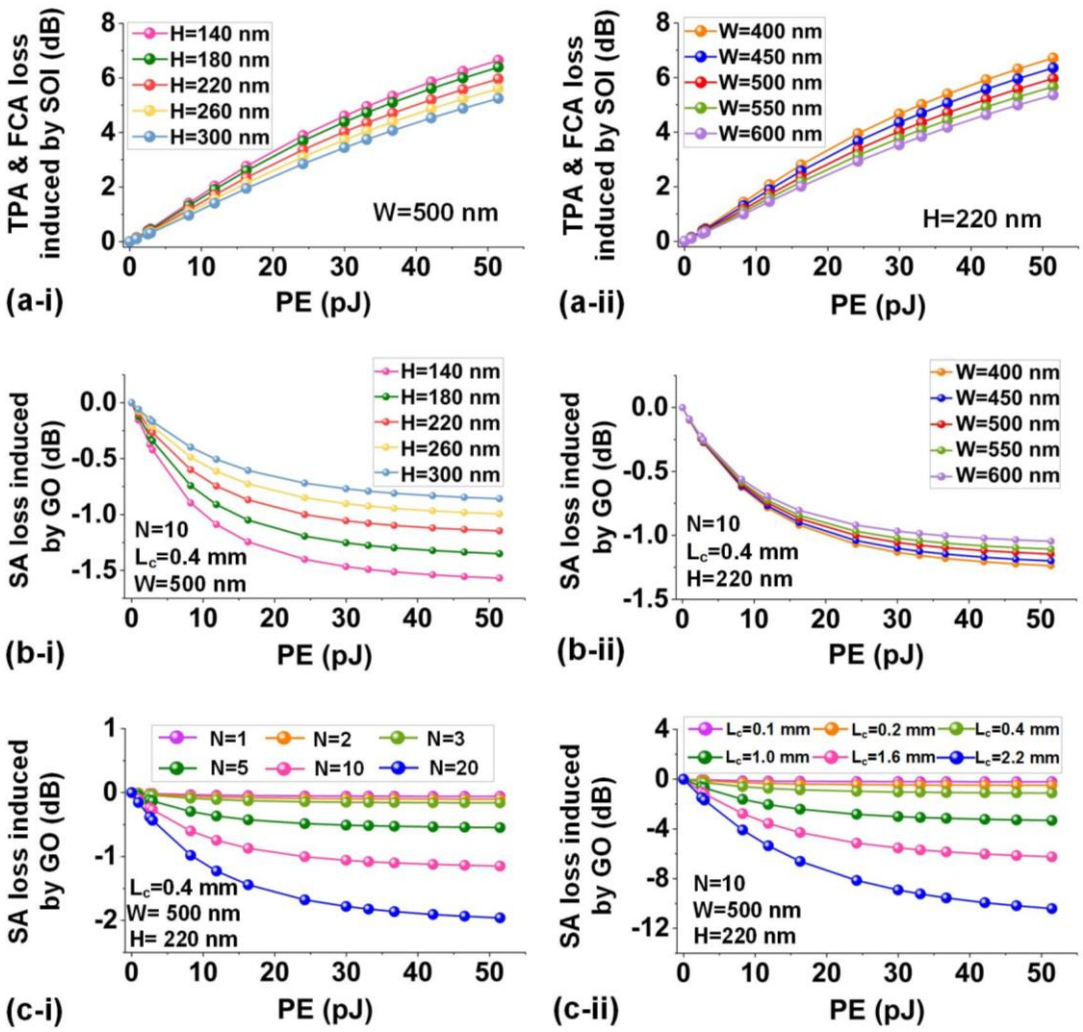

Figure 3. (a) Power-dependent TPA and FCA loss induced by bare SOI nanowires. (b) Power-dependent SA loss induced by GO films when N = 10, L_c = 0.4 mm, and L_0 = 1.3 mm. In (a) and (b), (i) and (ii) show the results for SOI nanowires with various H when W = 500 nm and various W when H = 220 nm, respectively. (c) Power-dependent SA loss induced by GO films for (i) various N when L_c = 0.4 mm and (ii) various L_c when N = 10. In (c), W = 500 nm, H = 220 nm, and L_0 = 1.3 mm. In (a) – (c), the total length of the bare SOI nanowires is 3 mm.

4. Nonlinear parameter and nonlinear FOM

In this section, we further investigate the influence of waveguide geometry (W and H) and GO film thickness (N) on the effective nonlinear parameter and nonlinear FOM. **Figures 4(a)** and **(b)** show the effective nonlinear parameter γ_{eff} versus layer number N, first for 5 different waveguide heights H at a fixed width W and then for 5 different widths W at a fixed height H. We plot the results for γ_{eff} for both (i) the absolute value and (ii) the relative value normalized to bare SOI nanowires with the same geometries. Note that, since γ_{eff} for the bare SOI nanowires is geometry dependent, the absolute γ_{eff} in (i) does not scale exactly as the relative γ_{eff} in (ii). In **Figure 4(c)**, we also plot the corresponding results for hybrid waveguides with the maximum, intermediate, and minimum waveguide dimensions amongst the 25 considered waveguide geometries (5 different H × 5 different W). The γ_{eff} 's were calculated based on [63, 65]

$$\gamma = \frac{2\pi}{\lambda} \frac{\iint_D n_0^2(x,y) n_2(x,y) S_z^2 dxdy}{\left[\iint_D n_0(x,y) S_z dxdy\right]^2} \tag{6}$$

where λ is the pulse central wavelength, D is the integral of the optical fields over different material regions, S_z is the time-averaged Poynting vector calculated using COMSOL Multiphysics, n_0 (x, y) and n_2 (x, y) are the linear refractive index and n_2 profiles over the waveguide cross section, respectively. We used n_2 (x, y) rather than the more general third-order nonlinearity ($\chi^{(3)}$) because the pulse spectral width (< 10 nm) is much smaller compared to the dispersion bandwidth of n_2. The values of n_2 for silica and silicon used in our calculation are 2.60 × 10^{-20} m^2/W [2] and 6 × 10^{-18} m^2/W, respectively, with the latter obtained by fitting experimental results for the bare SOI nanowires [68], which agrees with

other results [74]. The n_2 for layered GO, obtained from experimental results [48], decreases from 1.44 × 10 $^{-14}$ m^2/W for N = 1 to 1.24 × 10 $^{-14}$ for N = 20. We suggest that this mainly results from an increase in inhomogeneous defects and imperfect contact in thicker films. We neglect any changes in n_2 with pulse energy PE and wavelength since these parameters vary by much less than what these changes are observed for.

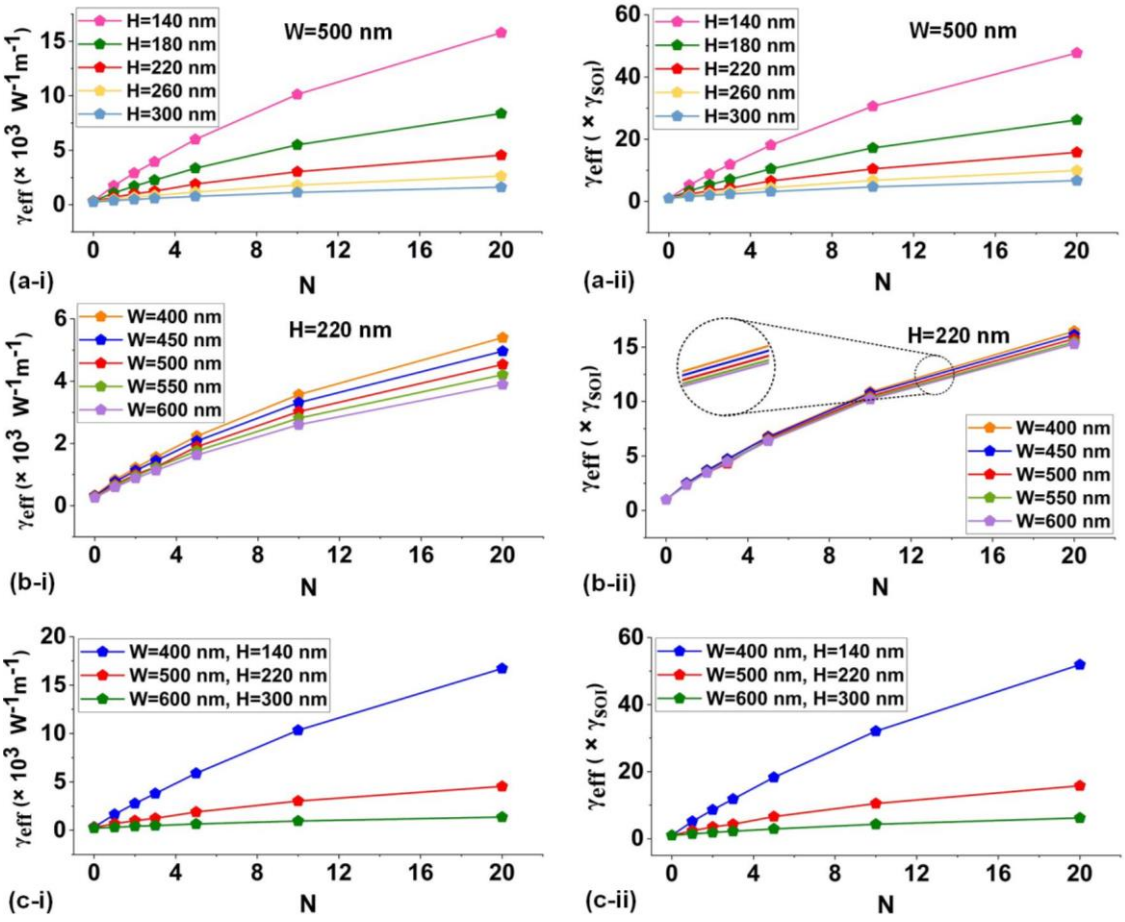

Figure 4. Effective nonlinear parameter (γ_{eff}) versus N for GO-coated SOI nanowires with (a) various H when W = 500 nm, (b) various W when H = 220 nm, and (c) the maximum, medium, and minimum waveguide dimensions. (i) shows the absolute γ_{eff} values and (ii) shows the relative γ_{eff} normalized to comparable bare SOI nanowires with the same waveguide geometries. The points at N = 0 correspond to the results for bare SOI nanowires.

In **Figures 4(a)** and **(b)**, γ_{eff} increases with layer number N and decreases with waveguide height H and width W, showing a similar trend to the propagation loss in **Figures 2(a)** and **(b)**. This indicates that an increased mode overlap leads to both an increased Kerr nonlinearity as well as linear loss. In **Figure 4(c)**, when N = 20, W = 400 nm, and H = 140 nm, a high γ_{eff} of 16711 W^{-1}m^{-1} is obtained, which is ≈52 times that of the associated bare SOI nanowire

(with the same waveguide geometry) and ≈4 times that of a comparable hybrid waveguide (with the same GO film thickness) with W = 500 nm and H = 220 nm. These results reflect the huge improvement in Kerr nonlinearity that can be obtained by not only introducing the GO films into SOI nanowires but by properly optimizing γ_{eff} by engineering the GO mode overlap.

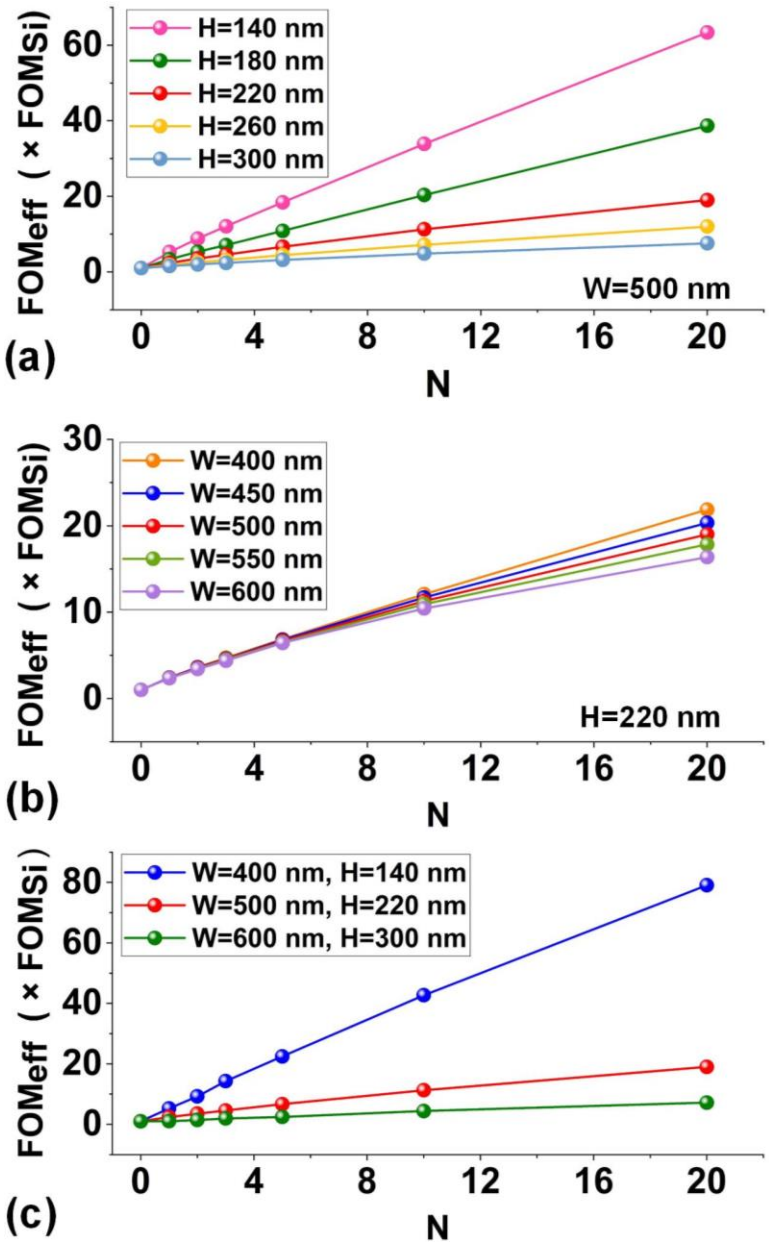

Figure 5. FOM_{eff} of the hybrid waveguides versus N for GO-coated SOI nanowires with (a) various H when W = 500 nm, (b) various W when H = 220 nm, and (c) the maximum, medium, and minimum waveguide dimensions. The points at N = 0 correspond to the results for bare SOI nanowires.

Based on the effective nonlinear parameter of the hybrid waveguides, we further investigate the effective nonlinear FOM (FOM_{eff}), which is widely used to quantitively characterize the

trade-off between the Kerr nonlinearity and nonlinear loss [2]. **Figures 5(a)** and **(b)** show the FOM_{eff} (normalized to the FOM of silicon) versus layer number N, first for different waveguide heights H at a fixed width W and then for different widths W with a fixed height H. The corresponding results for the hybrid waveguides with maximum, intermediate, and minimum waveguide dimensions are shown in **Figure 5(c)**. The FOM_{eff} 's were calculated by [1, 2]:

$$FOM_{eff} = \frac{n_{2,\,eff}}{\lambda_c \beta_{TPA,\,eff}} \tag{7}$$

where $\beta_{TPA,\,eff}$ is the effective TPA coefficient obtained by fitting the results in **Figures 3(b)** and **(c)** and $n_{2,\,eff}$ is the effective Kerr coefficient calculated from

$$n_{2,eff} = \frac{\lambda_c \gamma_{eff} A_{eff}}{2\pi} \tag{8}$$

where γ_{eff} is the effective nonlinear parameter in **Figure 4** and A_{eff} is the effective mode area. The $\beta_{TPA,\,eff}$'s are influenced by SA in the GO layers, which becomes more significant as the mode overlap increases. The SA decreases the overall absorption as the pulse energy PE increases, which acts oppositely to TPA and results in the effective $\beta_{TPA,\,eff}$'s of the hybrid waveguides being smaller than that of comparable bare SOI nanowires having the same waveguide geometries.

As shown in **Figure 5(c)**, the increased $n_{2,\,eff}$ and reduced $\beta_{TPA,\,eff}$ yield a high FOM_{eff} of 61 for N = 20, W = 400 nm, and H = 140 nm, which is ≈79 times that of silicon and ≈4 times that of a comparable hybrid waveguide (with the same GO film thickness) with W = 500 nm and H = 220 nm. Note that the FOM for bulk silicon reported in the literature varies by about a factor of 2. Our calculated FOM of ≈0.7 agrees with that in Ref. [74], which is slightly higher than other reported values [2]. The n_2 (6×10^{-18} m^2/W) and β_{TPA} (5×10^{-12} m/W) of silicon used in our calculations were obtained by fitting experimental results for the bare SOI nanowires [48]. In **Figures 5 (a)** and **(b),** the effective FOM increases with layer number N

and decreases with waveguide height H and width W, showing similar trends to the propagation loss in **Figure 2** and effective nonlinear parameter in **Figure 4**. This indicates that the nonlinear FOM can be improved by increasing the GO mode overlap via reducing the waveguide geometry or increasing the GO film thickness.

5. SPM-induced spectral broadening of optical pulses

Although the nonlinear FOM (**Eq. (7)**) has been widely used to characterize the Kerr nonlinear optical performance of bulk materials [2, 78], it does not represent the full picture. The nonlinear optical performance of hybrid waveguides incorporating 2D materials (or indeed for any device), must factor in the effects of the linear propagation loss [60]. For GO-coated SOI nanowires, the increased mode overlap yields an increased nonlinear FOM, but at the expense of an increased linear loss that sometimes can be significant. In this section, we examine SPM-induced spectral broadening of optical pulses to illustrate this trade-off. We show that, in addition to the waveguide geometry and GO film thickness, other parameters such as the GO film length and coating position are also very important to optimize the Kerr nonlinear performance.

Figure 6(a) compares the spectral broadening of optical pulses before and after propagating through both bare and GO-coated SOI nanowires, for various layer numbers N at fixed W = 500 nm, H = 220 nm, and L_c = 0.4 mm. The total length of the bare SOI nanowires is assumed to be 3 mm, as for previously fabricated devices [48]. To quantitatively analyse the spectral broadening, we use the broadening factor (BF) [48, 79, 80] defined as:

$$BF = \frac{\Delta\omega_{rms}}{\Delta\omega_0} \tag{9}$$

where $\Delta\omega_0$ and $\Delta\omega_{\mathrm{rms}}$ are the root-mean-square (RMS) spectral width of the input and output optical spectra, respectively.

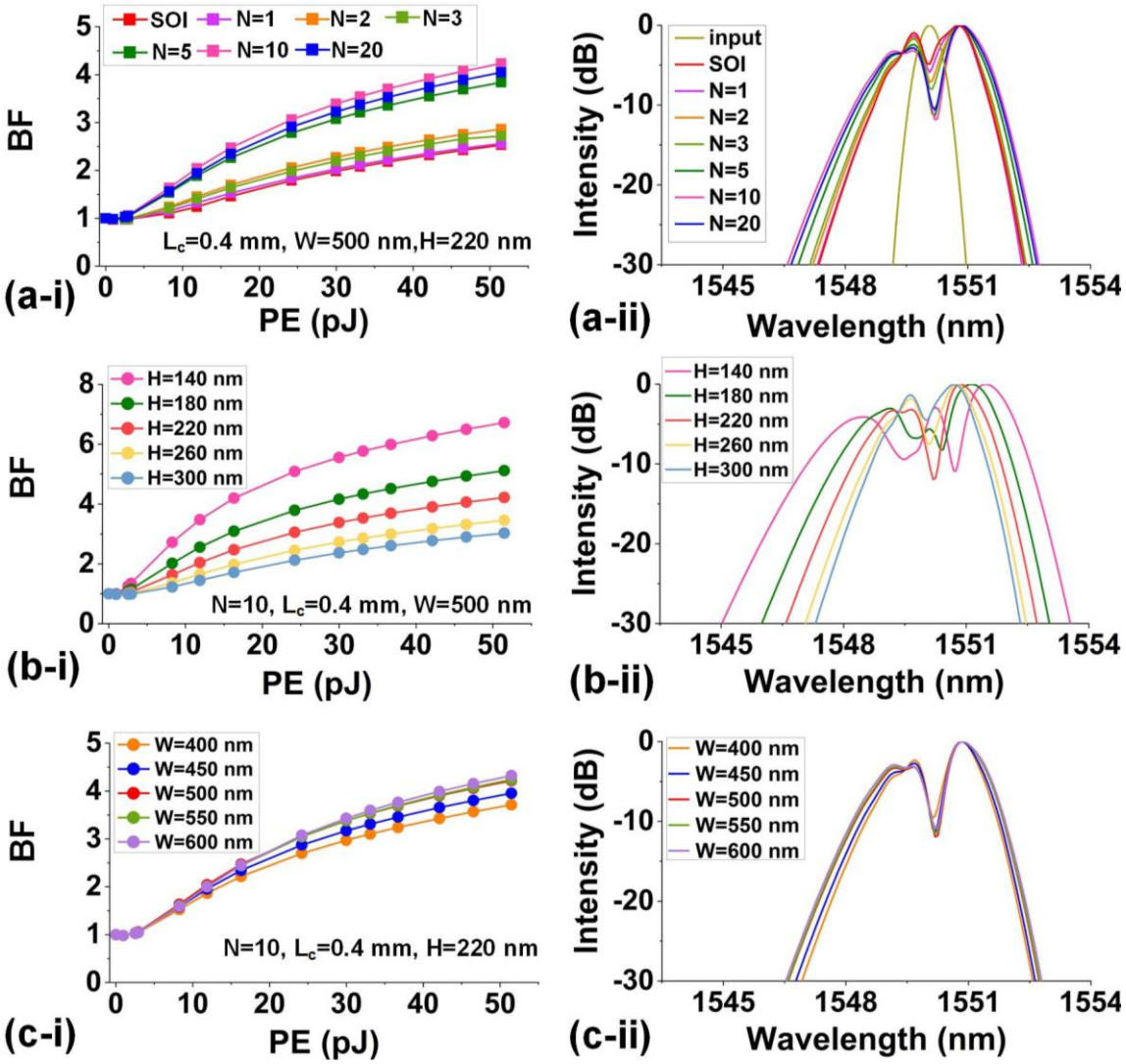

Figure 6. (a) Spectral broadening of optical pulses before and after going through bare and GO-coated SOI nanowires with various *N*. (b) − (c) Spectral broadening of optical pulses after going through GO-coated SOI nanowires for various *H* when *W* = 500 nm and various *W* when *H* = 220 nm, respectively. In (a) − (c), (i) shows BFs versus *PE* and (ii) shows the corresponding normalized spectra at *PE* = 51.5 pJ. In (a), *W* = 500 nm, *H* = 220 nm, and L_c = 0.4 mm. In (b) and (c), *N* = 10 and L_c = 0.4 mm. In (a) − (c), L_0 = 1.3 mm, and the total length of the bare SOI nanowires is 3 mm.

The spectral broadening was calculated using a split-step Fourier method to solve the nonlinear Schrödinger equation (NLSE) as follows [72, 74]:

$$\frac{\partial A}{\partial z} = -\frac{i\beta_2}{2}\frac{\partial^2 A}{\partial t^2} + i\gamma_{eff}|A|^2 A - \frac{1}{2}i\sigma\mu N_c A - \frac{1}{2}\alpha A \qquad (10)$$

where $i = \sqrt{1}$, β_2 is the second-order dispersion coefficient, μ is the free carrier dispersion (FCD) coefficient of silicon, and α is the total loss including both the linear loss (α_L) in **Figure 2** and the nonlinear loss in **Figure 3,** which can be expressed as:

$$\alpha = \alpha_L + \alpha_{TPA\text{-}Si} + \alpha_{FCA\text{-}Si} + \alpha_{SA\text{-}GO} \quad (11)$$

In our calculations, the hybrid waveguides were separated into bare and GO-coated segments. **Eq. (10)** was solved for each segment, with the output from the previous segment used as the input to the following segment. In **Figure 6(a)**, the hybrid waveguides show more significant spectral broadening than the bare SOI nanowires, with the maximum spectral broadening being achieved for an intermediate number of layers, N = 10. This results from the enhanced Kerr nonlinearity of the hybrid waveguides, balanced with the increased linear loss.

Figures 6(b) and **(c)** show the spectral broadening of optical pulses after propagation through bare and GO-coated SOI nanowires, for different waveguide geometries (H and W) but with the same GO film parameters (N = 10, L_c = 0.4 mm, and L_0 = 1.3 mm). The spectral broadening becomes more significant as H decreases, due to the significantly increased Kerr nonlinearity arising from the increased GO mode overlap, which dominates for the relatively short coating length considered here (i.e., L_c = 0.4 mm). On the other hand, the spectral broadening increases with W, showing the opposite trend to that of the FOM_{eff} in **Figure 5**. This could reflect the fact that the linear loss can become a limiting factor for the nonlinear performance of the hybrid waveguides – otherwise the maximum spectral broadening would have been achieved for the smallest W where the FOM_{eff} is the greatest. We also note that the broadened spectra exhibits a slight asymmetry, which is mainly induced by the FCA and FCD in silicon [74].

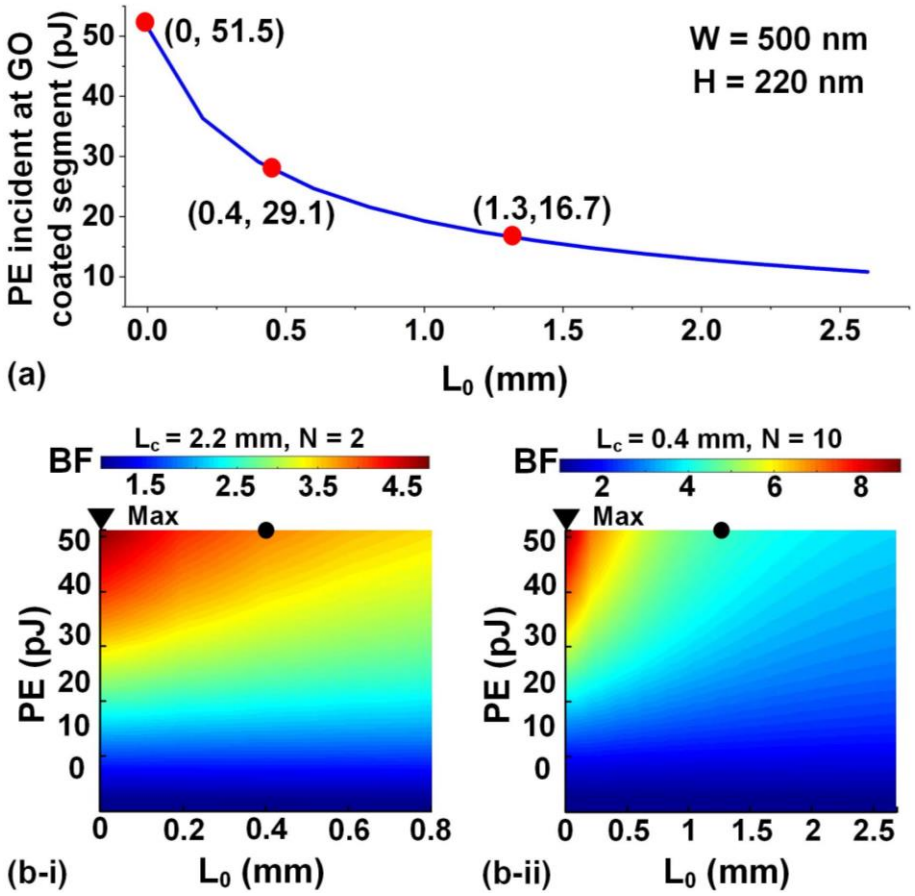

Figure 7. (a) *PE* incident at the GO-coated segment versus L_0. (b) BF of GO-coated SOI nanowires versus L_0 and *PE* when (i) L_c = 2.2 mm, N = 2 and (ii) L_c = 0.4 mm, N =10. The black points mark the BFs of 3.75 at L_0 = 0.4 mm, *PE*= 51.5 pJ in (i) and 4.34 at L_0 = 1.3 mm, *PE*= 51.5 pJ in (ii). In (a) and (b), W = 500 nm and H = 220 nm.

Figure 7(a) shows the pulse energy *PE* incident at the GO-coated segment as a function of coating position L_0. The *PE* decreases super-linearly with L_0, mainly induced by the super-linear increase in TPA and FCA of silicon. **Figure 7(b)** shows the BFs versus coating position L_0 and pulse energy *PE* when (i) L_c = 2.2 mm, N = 2 and (ii) L_c = 0.4 mm, N = 10. As expected, the spectral broadening becomes more significant as the *PE* increases, due to the increased nonlinear efficiency. On the other hand, the BFs decrease with L_0, with the maximum values (BF = 4.8 in **Figure 7(b-i)** and BF = 9.1 in **Figure 7(b-ii)**) being achieved at L_0 = 0 mm, where there is a maximum *PE* at the start of GO-coated segments. As marked in **Figures 7(b-i)** and **(b-ii)**, the BFs are 3.75 when L_0 = 0.4 mm, *PE* = 51.5 pJ and 4.34 when L_0 = 1.3 mm, *PE* = 51.5 pJ, showing good agreement with our previous experiments results [48]. In our previous experiments [48], windows were opened in the middle of the 3-mm-long SOI

nanowires, resulting in L_0 = 0.4 mm and L_0 = 1.3 mm for the devices with 2.2-mm-long and 0.4-mm-long opened windows. This was mainly out of consideration of device coupling loss – silica-clad waveguide regions were introduced between the inverse taper couplers and the opened windows to increase the coupling efficiency. Note that the difference induced by L_0 gets smaller for lower propagation loss of the bare waveguides, being much lower for Hydex and SiN waveguides [49, 63] versus SOI nanowires studied here.

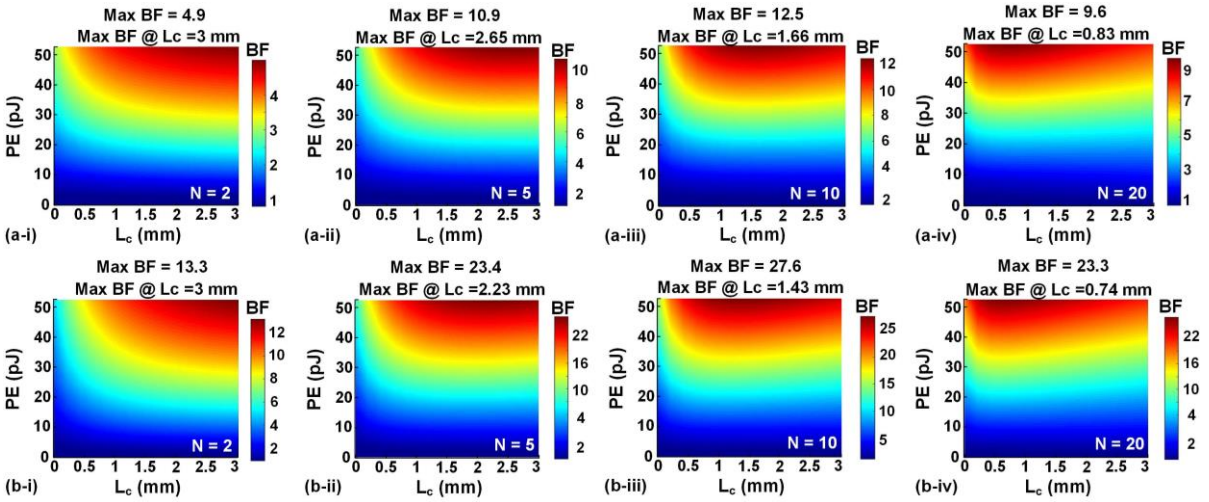

Figure 8. SPM BF of GO-coated SOI nanowires versus L_c and PE when (a) W = 500 nm, H = 220 nm and (b) W = 600 nm, H = 140 nm. (i) – (iv) show the results for N = 2, 5, 10, and 20, respectively. In (a) and (b), L_0 = 0 mm.

Figure 8(a) shows the BFs versus coating length L_c and pulse energy PE when (i) N = 2, (ii) N = 5, (iii) N = 10, and (iv) N = 20, respectively, with the other device parameters kept constant (L_0 = 0 mm, W = 500 nm, and H = 220 nm). The maximum BFs are achieved for L_c = 3 mm, 1.66 mm, and 0.83 mm, respectively, which shifts towards shorter lengths as N increases, following the trend also seen with the layer number N in **Figure 6(a)**. This reflects the fact that the enhancement in the Kerr nonlinearity dominates for hybrid waveguides with relatively small L_c and N, while the influence of the loss increase become more significant as L_c and N increase. A maximum BF of 12.5 is achieved when N = 10 and L_c = 1.66 mm, reflecting that there is still room for improvement on the basis of the maximum BF in **Figure 7(b)** (i.e., 9.1) by optimizing the GO film length. **Figure 8(b)** depicts the corresponding results for the hybrid waveguides with W = 600 nm and H = 140 nm, which shows the best

spectral broadening among 25 different waveguide geometries considered in our study. A maximum BF of 27.6 is achieved when $N = 10$ and $L_c = 1.43$ mm, which is ≈2.2 times higher than the maximum BF in **Figure 8(a)** and more than 6 times higher than previous experiments [48], reflecting the potential for improvement by optimizing the waveguide geometry.

6. Discussion

In this section, we consider the influence of loss, pulse chirp, material anisotropy, and the interplay between SA and SPM on the Kerr nonlinear performance. **Figure 9(a)** shows the loss for optical pulses after propagation through hybrid waveguides, factoring in α_L, α_L and $\alpha_{TPA\text{-}Si}$, the overall loss excluding $\alpha_{SA\text{-}GO}$, and the total overall loss, calculated from **Eqs. (3) – (5)**. The corresponding BFs and pulse spectra calculated from **Eqs. (9) – (11)** are shown in **Figures 9(b)** and **(c)**, respectively. The loss remains constant when considering only α_L but increases with pulse energy PE when including $\alpha_{TPA\text{-}Si}$ and $\alpha_{FCA\text{-}Si}$. We neglect any variation in α_L with PE for the hybrid waveguides, due to the much weaker photo-thermal changes of GO induced by picosecond optical pulses, with much lower average power than the continuous-wave pump for FWM [49, 65]. After including $\alpha_{SA\text{-}GO}$, the overall loss decreases, enhancing the SPM and spectral broadening. In **Figure 9(c)**, although the intrinsic TPA itself leaves the pulse spectrum symmetric, the resulting FCA makes it considerably asymmetric.

While the linear loss of the layered GO films does pose a limitation for the Kerr nonlinear performance of the hybrid waveguide, as mentioned, it is not a fundamental material property, and any reduction by optimizing the film fabrication processes would improve the performance further. **Figure 9(d)** shows the linear propagation loss and BF of the hybrid waveguides versus GO extinction coefficient k. For the GO film with the state-of-the art k = 0.0089 (for N = 10), the corresponding propagation loss and BF are 15.8 dB/mm and 4.34, respectively, in good agreement with experiments [48]. When k decreases to 0.0008, the BF increases to 6.30 – a factor of ≈1.5 higher than the BF for k = 0.0089. Note that the GO coating length here (L_c = 0.4 mm) is relatively short, and so the influence of the loss of the GO films is not very significant. For the hybrid waveguide in **Figure 6 (b-iii)** with a longer GO coating length of L_c = 1.43 mm, the BF increases from 27.6 (for k = 0.0089) to 70 (for k =

0.0008), highlighting the strong potential for improving the nonlinear performance by reducing the GO film linear loss.

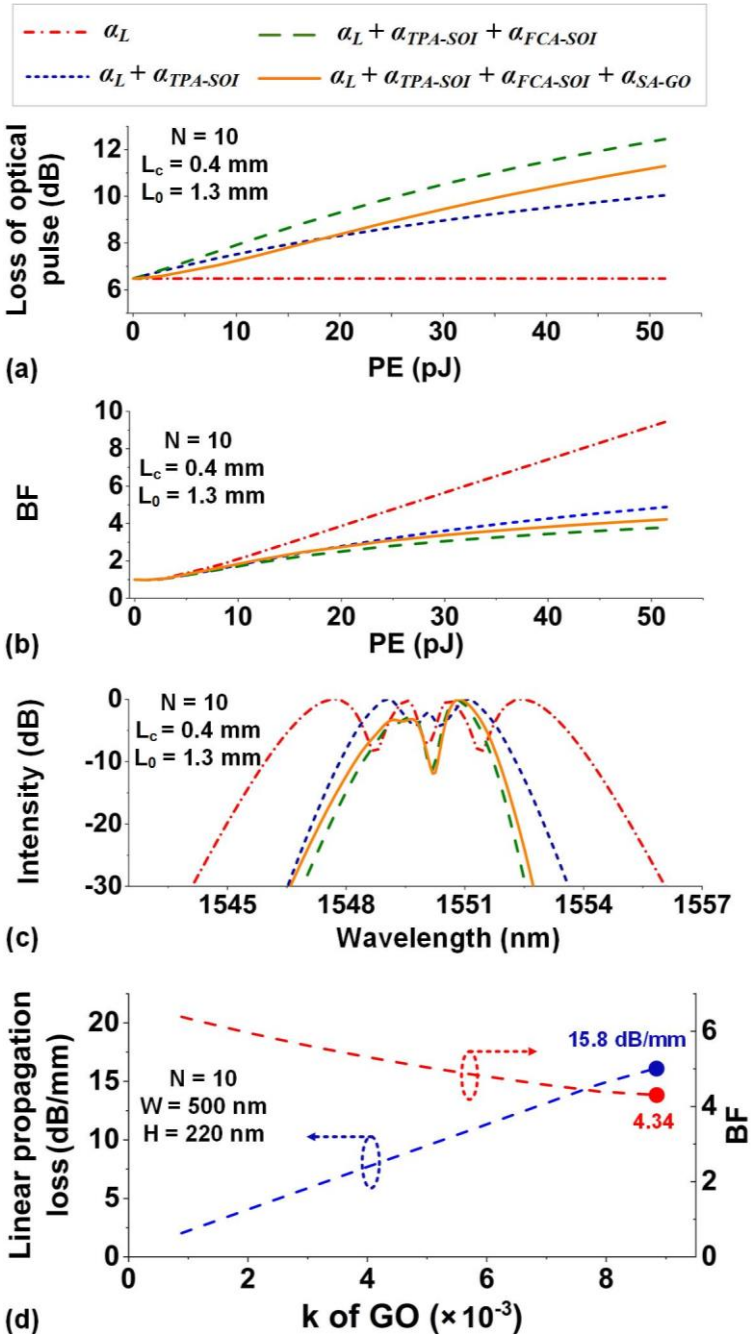

Figure 9. (a) Loss of optical pulses after going through GO-coated SOI nanowires when considering α_L (dotted curves), α_L and $\alpha_{TPA\text{-}SOI}$ (short-dashed curves), overall loss except for $\alpha_{SA\text{-}GO}$ (dashed curves), and overall loss (solid curves). (b) BFs calculated based on the loss in (a). (c) Normalized spectra at PE = 51.5 pJ. (d) The linear waveguide propagation loss and BF of GO-coated SOI nanowires versus extinction coefficient k of GO. The points at k = 0.0089 refer to the state-of-the-art values in Ref. [48]. In (a) – (d), the device parameters are W = 500 nm, H = 220 nm, N = 10, L_c = 0.4 mm, and L_0 = 1.3 mm.

Figure 10(a) plots the mode overlap with the GO film (η) versus layer number N. Most of the power is confined to the SOI nanowires rather than the GO film (< 6% for N = 20), mainly

due to the larger cross sectional area of the SOI nanowires compared to the ultrathin 2D GO films. In **Figure 10(a)**, we show the ratio of the power in the GO on both sidewalls to the power in entire film, which is < 3% and decreases with N. This indicates that the TE mode overlap with GO on both waveguide sidewalls is negligible compared with that for GO on the waveguide top, and so we use the in-plane n_2 of GO (corresponding to TE polarization) in our calculations, neglecting any anisotropy in n_2 of the 2D layered GO films.

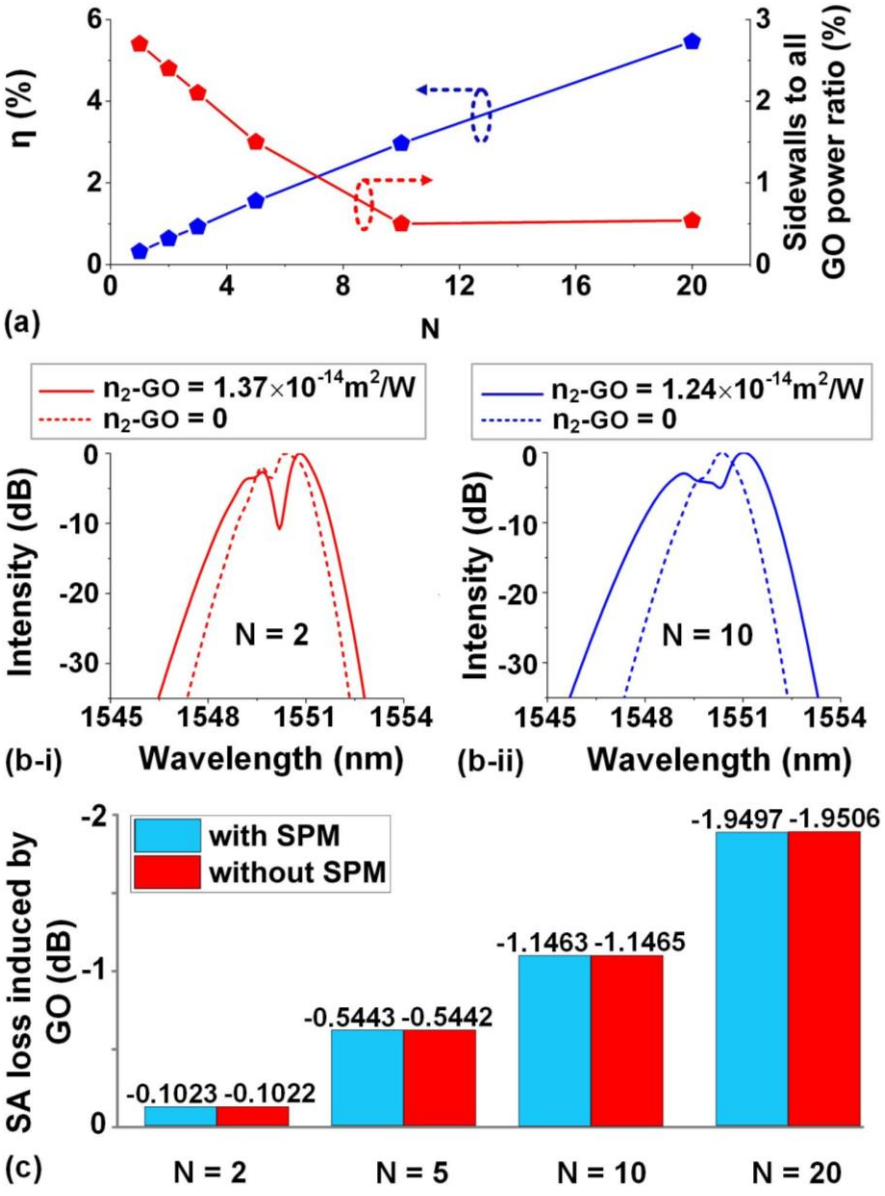

Figure 10. (a) GO mode overlap and ratio of power in GO coated on both sidewalls to that in all GO material regions versus N. (b) Comparison of optical pulse spectra after going through GO-coated SOI nanowires with (i) $N = 2$ when $n_{2\text{-GO}} = 0$ and $n_{2\text{-GO}} = 1.37 \times 10^{-14}$ m^2/W (ii) $N = 10$ when $n_{2\text{-GO}} = 0$ and $n_{2\text{-GO}} = 1.24 \times 10^{-14}$ m^2/W. (c) Comparison of SA loss of the hybrid waveguides with and without considering spectral broadening induced by GO. In (a), (b), and (c), $W = 500$ nm, $H = 220$ nm, $L_c = 0.4$ mm, and $L_0 = 1.3$ mm.

Figure 10(b) shows the optical pulse spectra after propagation through the hybrid waveguides with N = 2 and N = 10**,** respectively. The solid curves show the results based on the experimentally measured n_2 of GO (which varies slightly with N), whereas the dashed curves were calculated neglecting the contribution of the GO film to the SPM (i.e., assuming the n_2 of GO is 0). **Figure 10(c)** compares the corresponding SA loss of the hybrid waveguides. The maximum difference between them is < 0.2%, reflecting that the influence of SPM on SA is negligible. This is mainly because the total length of the hybrid waveguides (3 mm) was much shorter than the dispersion length (> 1 m), and so any change in the pulse spectrum induced by SPM did not significantly affect the temporal pulse shape [79].

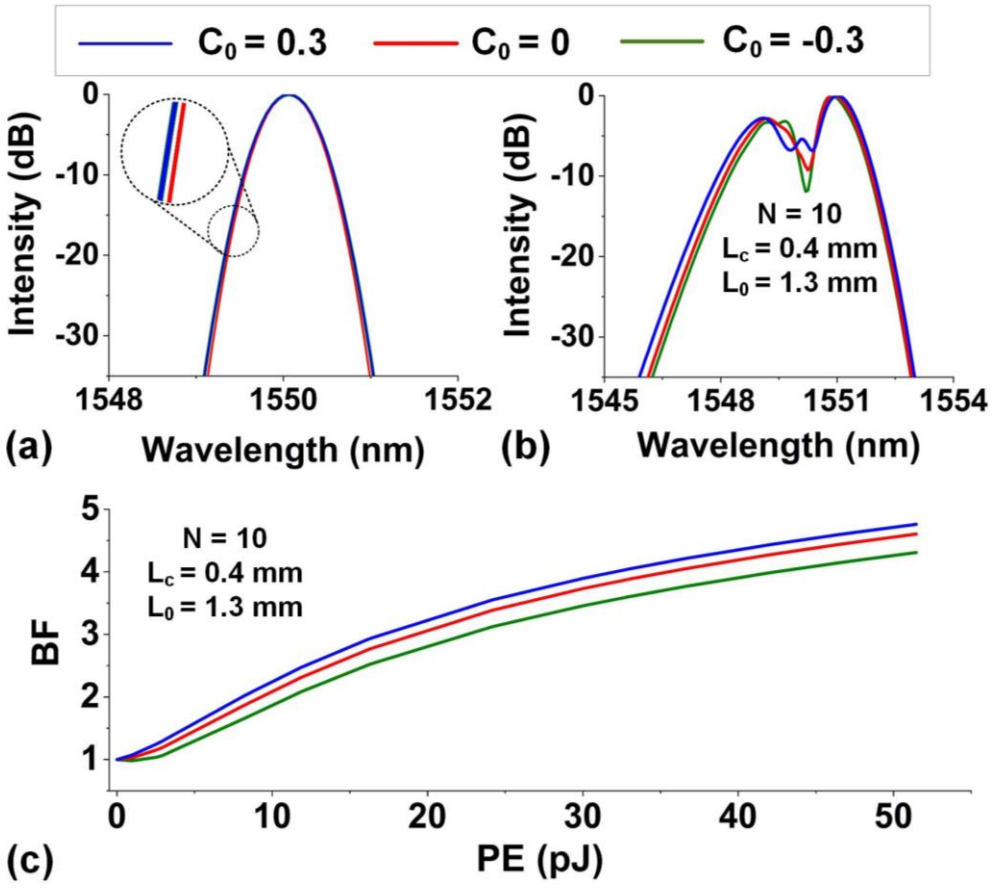

Figure 11. Spectral broadening of optical pulses before and after going through GO-coated SOI nanowires for various C_0. (a) Input pulse spectra. (b) Normalized spectra at PE = 51.5 pJ. (c) BFs versus PE. In (b) and (c), W = 500 nm, H = 220 nm, N = 10, L_c = 0.4 mm, and L_0 = 1.3 m.

Figure 11 compares the SPM performance for input optical pulses versus chirp parameter C_0. The pulse width T as a function of C_0 is given by:

$$T = \frac{T_0}{(1+C_0^2)^{1/2}} \tag{12}$$

In **Figure. 11(a)**, the input pulse spectra for the same absolute value of chirp (0.3) but with opposite signs overlap each other, in agreement with **Eq. (12)**. The corresponding pulse spectra and BFs are shown in **Figures 11(b)** and **(c)**, respectively. Compared with unchirped pulses (i.e., $C_0 = 0$), the spectral broadening increases when $C_0 > 0$ but decreases when $C_0 < 0$, since the positive chirp induced by SPM adds to a positive C_0 , while it is offset by a negative C_0.

7. Conclusion

In summary, we theoretically investigate and optimize the Kerr nonlinear optical performance of SOI nanowires integrated with 2D layered GO films. Detailed analysis of the influence of waveguide geometry and GO film thickness on the propagation loss, nonlinear parameter, and nonlinear FOM is performed. We show that the effective nonlinear parameter and nonlinear FOM can be increased by up to ≈52 and ≈79 times relative to bare SOI nanowires, respectively. To examine the trade-off between increasing the Kerr nonlinearity and minimizing linear loss, we consider SPM-induced spectral broadening of optical pulses. We show that a high BF of 27.6 can be achieved by properly balancing this trade-off, more than a factor of 6 higher than what has been achieved experimentally. Finally, the role of pulse chirp, material anisotropy, and the interplay between SA and SPM in SPM-induced spectral broadening is also investigated. These results highlight the significant potential of GO films to enhance the Kerr nonlinear optical performance of SOI nanowires for practical applications.

Acknowledgements

This work was supported by the Australian Research Council Discovery Projects Programs (No. DP150102972 and DP190103186), the Swinburne ECR-SUPRA program, the Industrial Transformation Training Centres scheme (Grant No. IC180100005), and the Beijing Natural Science Foundation (No. Z180007).

Received: (will be filled in by the editorial staff)

Revised: (will be filled in by the editorial staff)
Published online: (will be filled in by the editorial staff)

References

1. J. Leuthold, C. Koos, W. Freude, *Nat. Photonics* **2010**, *4*, 535.
2. D. J. Moss, R. Morandotti, A. L. Gaeta, M. Lipson, *Nat. Photonics* **2013**, *7*, 597.
3. M. A. Foster, R. Salem, D. F. Geraghty, A. C. T. Foster, M. Lipson, A. L. Gaeta, *Nature* **2008**, *456*, 81.
4. M. P. Nielsen, X. Shi, P. Dichtl, S. A. Maier, R. F. Oulton, *Science* **2017**, *358*, 1179.
5. C. Koos, P. Vorreau, T. Vallaitis, P. Dumon, W. Bogaerts, R. Baets, B. Esembeson, I. Biaggio, T. Michinobu, F. Diederich, W. Freude, J. Leuthold, *Nat. Photonics* **2009**, *3*, 216.
6. B. Corcoran, M. Tan, X. Xu, A. Boes, J. Wu, T. G. Nguyen, S. T. Chu, B. E. Little, R. Morandotti, A. Mitchell, D. J. Moss, *Nat. Commun.* **2020**, *11*, 2568.
7. S. T. Cundiff, *Nature* **2007**, *450*, 1175.
8. J. K. Jang, M. Erkintalo, S. G. Murdoch, S. Coen, *Nat. Photonics* **2013**, *7*, 657.
9. A. Martínez, J. Blasco, P. Sanchis, J. V. Galán, J.G. Rupérez, E. Jordana, P. Gautier, Y. Lebour, S. Hernández, R. Spano, R. Guider, N. Daldosso, B. Garrido, J. M. Fedeli, L. Pavesi, J. Martí, *Nano Lett.* **2010**, *10*, 1506.
10. D. M. Lukin, C. Dory, M. A. Guidry, K. Y. Yang, S. D. Mishra, R. Trivedi, M. Radulaski, S. Sun, D. Vercruysse, G. H. Ahn, J. Vučković, *Nat. Photonics* **2020**, *14*, 330.
11. E. A. Kittlaus, H. Shin, P. T. Rakich, *Nat. Photonics* **2016**, *10*, 463.
12. H. Guo, C. Herkommer, A. Billat, D. Grassani, C. Zhang, M. H. P. Pfeiffer, W. Weng, C. S. Brès, T. J. Kippenberg, *Nat. Photonics* **2018**, *12*, 330.
13. N. Singh, D. D. Hudson, Y. Yu, C. Grillet, S. D. Jackson, A. C. Bedoya, A. Read, P.Atanackovic, S. G. Duvall, S. Palomba, B. L. Davies, S. Madden, D. J. Moss, B. J. Eggleton, *Optica* **2015**, *2*, 797.
14. D. Dai, L. Liu, S. Gao, D. X. Xu, S. He, *Laser Photonics Rev.* **2013**, *7*, 303.
15. S. Feng, T. Lei, H. Chen, H. Cai, X. Luo, A. W. Poon, *Laser Photonics Rev.* **2012**, *6*, 145.
16. W. Liu, M. Li, R. S. Guzzon, E. J. Norberg, J. S. Parker, M. Lu, L. A. Coldren, J. Yao, *Nat. Photonics* **2016**, *10*, 190.
17. W. Bogaerts, D. Pérez, J. Capmany, D. A. B. Miller, J. Poon, D. Englund, F. Morichetti, A. Melloni, *Nature* **2020**, *586*, 207.
18. P.Cheben, R. Halir, J. H. Schmid, H. A. Atwater, D. R. Smith, *Nature* **2018**, *560*, 565.
19. W. Bogaerts, L. Chrostowski, *Laser Photonics Rev.* **2018**, *12*, 1700237.
20. A. G. Griffith, R. K. Lau, J. Cardenas, Y. Okawachi, A. Mohanty, R. Fain, Y. H. Lee, M. Yu, C. T. Phare, C. B. Poitras, A. L. Gaeta, M. Lipson, *Nat. Commun.* **2015**, *6*, 6299.
21. D. J. Moss, et al., "Ultrafast all-optical modulation via two-photon absorption in silicon-insulator waveguides," Electronics Letters, vol. 41, no. 6, pp. 320-321, 2005. DOI:10.1049/el:20058051
22. M. R. E. Lamont, et al.,"Two-photon absorption effects on self-phase-modulation-based 2R optical regeneration," Photonics Technology Letters, vol. 18, no. 10, pp. 1185-1187, 2006. DOI:10.1109/LPT.2006.874718.

23. A.Tuniz, G. Brawley, D. J. Moss, and B. J. Eggleton, "Two-photon absorption effects on Raman gain in single mode As2Se3 chalcogenide glass fiber," Optics Express, vol. 16, no. 22, pp. 18524-18534, 2008. DOI: 10.1364/OE.16.018524.
24. M. H. P. Pfeiffer, A. Kordts, V. Brasch, M. Zervas, M. Geiselmann, J. D. Jost, T. J. Kippenberg, *Optica* **2016**, *3*, 20.
25. J. S. Levy, A. Gondarenko, M. A. Foster, A. C. T. Foster, A. L. Gaeta, M. Lipson, *Nat. Photonics* **2010,** *4*, 37.
26. M. Ferrera, L. Razzari, D. Duchesne, R. Morandotti, Z. Yang, M. Liscidini, J. E. Sipe, S. Chu, B. E. Little, D. J. Moss, *Nat. Photonics* **2008**, *2*, 737.
27. L. Razzari, D. Duchesne, M. Ferrera, R. Morandotti, S. Chu, B. E. Little, D. J. Moss, *Nat. Photonics* **2010**, *4*, 41.
28. J. Wu, X. Xu, T. G. Nguyen, S. T. Chu, B. E. Little, R. Morandotti, A. Mitchell, D. J. Moss, *IEEE J. Sel. Top. Quantum Electron*. **2018**, *24*, 1.
29. A. Pasquazi, et al., "Sub-picosecond phase-sensitive optical pulse characterization on a chip", Nature Photonics, vol. 5, no. 10, pp. 618-623 (2011). DOI: 10.1038/nphoton.2011.199.
30. D. Duchesne, M. Peccianti, M. R. E. Lamont, et al., "Supercontinuum generation in a high index doped silica glass spiral waveguide," Optics Express, vol. 18, no, 2, pp. 923-930, 2010.
31. M. Ferrera, et al., "On-chip CMOS-compatible all-optical integrator", Nature Communications, vol. 1, Article 29, 2010. DOI:10.1038/ncomms1028
32. H.Bao, et al., "Turing patterns in a fibre laser with a nested micro-resonator: robust and controllable micro-comb generation", Physical Review Research, vol. 2, 023395 (2020). DOI: 10.1103/PhysRevResearch.00.003000.
33. A. Pasquazi, Y. Park, J. Azana, et al., "Efficient wavelength conversion and net parametric gain via Four Wave Mixing in a high index doped silica waveguide," Optics Express, vol. 18, no. 8, pp. 7634-7641, 2010.
34. M. Peccianti, M. Ferrera, L. Razzari, et al., "Subpicosecond optical pulse compression via an integrated nonlinear chirper," Optics Express, vol. 18, no. 8, pp. 7625-7633, 2010.
35. D. Duchesne, M. Ferrera, L. Razzari, et al., "Efficient self-phase modulation in low loss, high index doped silica glass integrated waveguides," Optics Express, vol. 17, no. 3, pp. 1865-1870, 2009.
36. A. Pasquazi, M. Peccianti, L. Razzari, D. J. Moss, S. Coen, M. Erkintalo, Y. K. Chembo, T. Hansson, S. Wabnitz, P. Del'Haye, X. X. Xue, A. M. Weiner, and R. Morandotti, "Micro-combs: A novel generation of optical sources," Physics Reports, vol. 729, pp. 1-81, Jan 27. 2018.
37. M. Peccianti, et al., "Demonstration of an ultrafast nonlinear microcavity modelocked laser", Nature Communications, vol. 3, pp. 765, 2012. DOI:10.1038/ncomms1762
38. M. Kues, et al., "Passively modelocked laser with an ultra-narrow spectral width", Nature Photonics, vol. 11, no. 3, pp. 159, 2017. DOI:10.1038/nphoton.2016.271
39. A. Pasquazi, L. Caspani, M. Peccianti, et al., "Self-locked optical parametric oscillation in a CMOS compatible microring resonator: a route to robust optical frequency comb generation on a chip," Optics Express, vol. 21, no. 11, pp. 13333-13341, 2013.
40. C. Reimer, et al., "Cross-polarized photon-pair generation and bi-chromatically pumped optical parametric oscillation on a chip", Nature Communications, vol. 6, Article 8236, 2015. DOI: 10.1038/ncomms9236
41. C. Reimer, M. Kues, P. Roztocki, B. Wetzel, F. Grazioso, B. E. Little, S. T. Chu, T. Johnston, Y. Bromberg, L. Caspani, D. J. Moss, and R. Morandotti, "Generation of

multiphoton entangled quantum states by means of integrated frequency combs," Science, vol. 351, no. 6278, pp. 1176-1180, 2016.
42. M. Kues, et al., "On-chip generation of high-dimensional entangled quantum states and their coherent control", Nature, vol. 546, no. 7660, pp. 622-626, 2017.
43. P. Roztocki, M. Kues, C. Reimer, B. Wetzel, S. Sciara, Y. Zhang, A. Cino, B. E. Little, S. T. Chu, D. J. Moss, and R. Morandotti, "Practical system for the generation of pulsed quantum frequency combs," Optics Express, vol. 25, no. 16, pp. 18940-18949, 2017.
44. M. Kues, C. Reimer, A. Weiner, J. Lukens, W. Munro, D. J. Moss, and R. Morandotti, "Quantum Optical Micro-combs", Nature Photonics, vol. 13, no.3, pp. 170-179, 2019.
45. C. Reimer, et al.,"High-dimensional one-way quantum processing implemented on d-level cluster states", Nature Physics, vol. 15, no.2, pp. 148–153, 2019.
46. T. Gu, N. Petrone, J. F. McMillan, A. van der Zande, M. Yu, G. Q. Lo, D. L. Kwong, J. Hone, C. W. Wong, *Nat. Photonics* **2012**, *6*, 554.
47. T. Jiang, D. Huang, J. Cheng, X. Fan, Z. Zhang, Y. Shan, Y. Yi, Y. Dai, L. Shi, K. Liu, C. Zeng, J. Zi, J. E. Sipe, Y. R. Shen, W. T. Liu, S. Wu, *Nat. Photonics* **2018**, *12*, 430.
48. Y. Zhang, J. Wu, Y. Yang, Y. Qu, L. Jia, T. Moein, B. Jia, D. J. Moss, *ACS Appl. Mater. Interfaces* **2020**, *12*, 33094.
49. Y. Qu, J. Wu, Y. Yang, Y. Zhang, Y. Liang, H. E. Dirani, R. Crochemore, P. Demongodin, C. Sciancalepore, C. Grillet, C. Monat, B. Jia, D. J. Moss, *Adv. Opt. Mater*. **2020,** *8*, 2001048.
50. P. C. Debnath, K. Park, Y. W. Song, *Small Methods* **2018**, *2*, 1700315.
51. S. Uddin, P. C. Debnath, K. Park, Y. W. Song, *Sci. Rep*. **2017**, *7*, 43371.
52. L. Liu, K. Xu, X. Wan, J. Xu, C. Y. Wong, H. K. Tsang, *Photonics Res*. **2015**, *3*, 206.
53. Y. Zhang, L. Tao, D. Yi, J. B. Xu, H. K. Tsang, *J. Opt*. **2020**, *22*, 025503.
54. K. P. Loh, Q. Bao, G. Eda, M. Chhowalla, *Nat. Chem*. **2010,** *2*, 1015.
55. X. Li, H. Ren, X. Chen, J. Liu, Q. Li, C. Li, G. Xue, J. Jia, L. Cao, A. Sahu, B. Hu, Y. Wang, G. Jin, M. Gu, *Nat. Commun*. **2015**, *6*, 6984.
56. X. Zheng, B. Jia, H. Lin, L. Qiu, D. Li, M. Gu, *Nat. Commun*. **2015**, *6*, 8433.
57. H. Lin, B. C. P. Sturmberg, K. T. Lin, Y. Yang, X. Zheng, T. K. Chong, C. M. de Sterke, B. Jia, *Nat. Photonics* **2019**, *13*, 270.
58. X. Zheng, B. Jia, X. Chen, M. Gu, *Adv. Mater*. **2014**, *26*, 2699.
59. K. T. Lin, H. Lin, T. Yang, B. Jia, *Nat. Commun*. **2020**, *11*, 1389.
60. J. Wu, L. Jia, Y. Zhang, Y. Qu, B. Jia, D. J. Moss, "Graphene oxide for integrated photonics and flat optics," *Adv. Mater.* **2020**. in press. Preprint: https://www.preprints.org/manuscript/202009.0492/v1
61. X. Xu, X. Zheng, F. He, Z. Wang, H. Subbaraman, Y. Wang, B. Jia, R. T. Chen, *Sci. Rep*. **2017**, *7*, 9646.
62. Y. Yang, H. Lin, B. Y. Zhang, Y. Zhang, X. Zheng, A. Yu, M. Hong, B. Jia, *ACS Photonics* **2019**, *6*, 1033.
63. Y. Yang, J. Wu, X. Xu, Y. Liang, S. T. Chu, B. E. Little, R. Morandotti, B. Jia, D. J. Moss, *APL Photonics* **2018**, *3*, 120803.
64. L. Guo, R. Q. Shao, Y. L. Zhang, H. B. Jiang, X. B. Li, S. Y. Xie, B. B. Xu, Q. D. Chen, J. F. Song, H. B. Sun, *J. Phys. Chem. C* **2012**, *116*, 3594.
65. J. Wu, Y. Yang, Y. Qu, L. Jia, Y. Zhang, X. Xu, S. T. Chu, B. E. Little, R. Morandotti, B. Jia, D. J. Moss, *Small* **2020**, *16*, 1906563.
66. J. Wu, Y. Yang, Y. Qu, X. Xu, Y. Liang, S. T. Chu, B. E. Little, R. Morandotti, B. Jia, D. J. Moss, *Laser Photon. Rev*. **2019**, *13*, 1900056.
67. M. Liu, X. Yin, E. U. Avila, B. Geng, T. Zentgraf, L. Ju, F. Wang, X. Zhang, *Nature* **2011**, *474*, 64.

68. H. Lin, Y. Song, Y. Huang, D. Kita, S. D. Jones, K. Wang, L. Li, J. Li, H. Zheng, Z. Luo, H. Wang, S. Novak, A. Yadav, C. C. Huang, R. J. Shiue, D. Englund, T. Gu, D. Hewak, K. Richardson, J. Kong, J. Hu, *Nat. Photonics* **2017**, *11*, 798.
69. M. F. E. Kady, V. Strong, S. Dubin, R. B. Kaner, *Science* **2012**, *335*, 1326.
70. Y. Su, Y. Zhang, C. Qiu, X. Guo, L. Sun, *Adv. Mater. Technol.* **2020**, *5*, 1901153.
71. L. Liu, K. Xu, X. Wan, J. Xu, C. Y. Wong, H. K. Tsang, *Photonics Res.* **2015**, *3*, 206.
72. Q. Feng, H. Cong, B. Zhang, W. Wei, Y. Liang, S. Fang, T. Wang, J. Zhang, *Appl. Phys. Lett.* **2019**, *114*, 071104.
73. J. Wu, P. Cao, T. Pan, Y. Yang, C. Qiu, C. Tremblay, Y. Su, *Photonics Res.* **2014**, *3*, 9.
74. L. Yin, G. P. Agrawal, *Opt. Lett.* **2007**, *32*, 2031.
75. X. Li, Y. Tang, Z. Yan, Y. Wang, B. Meng, G. Liang, H. Sun, X. Yu, Y. Zhang, X. Cheng, Q. J. Wang, *IEEE J. Sel. Top. Quantum Electron.* **2014**, *20*, 441.
76. D. Chemla, D. Miller, P. Smith, A. Gossard, W. Wiegmann, *IEEE J. Quantum Electron.* **1984**, *20*, 265.
77. Q. Bao, H. Zhang, Y. Wang, Z. Ni, Y. Yan, Z. X. Shen, K. P. Loh, D. Y. Tang, *Adv. Func. Mater.* **2009**, *19*, 3077.
78. V. Mizrahi, K. W. DeLong, G. I. Stegeman, M. A. Saifi, M. J. Andrejco, *Opt. Lett.* **1989**, *14*, 1140.
79. P. Demongodin, H. E.Dirani, J. Lhuillier, R. Crochemore, M. Kemiche, T. Wood, S. Callard, P. R. Romeo, C. Sciancalepore, C. Grillet, C. Monat, *APL Photonics* **2019**, *4*, 076102.
80. N. Vermeulen, D. C. Lurbe, M. Khoder, I. Pasternak, A. Krajewska, T. Ciuk, W. Strupinski, J. Cheng, H. Thienpont, J. V. Erps, *Nat. Commun.* **2018**, *9*, 2675.